Contents lists available at ScienceDirect

Electric Power Systems Research

journal homepage: www.elsevier.com

Accurate aggregated modelling of wind farm systems in modified sequence domain for stability analysis

Haoxiang Zong [a], Jing Lyu [a], Xu Cai [a, *], Chen Zhang [b], Marta Molinas [b], Fangquan Rao [a]

[a] Wind Power Research Centre, Shanghai Jiao Tong University, Shanghai, China
[b] Department of Engineering Cybernetics, Norwegian University of Science and Technology, Trondheim, Norway

ARTICLE INFO

Keywords:
Wind farm
Stability
Sequence coupling
Modified sequence impedance
Frequency domain
Inertia

ABSTRACT

With the wind power penetration rate continuously rising, a suitable wind farm model considering both accuracy and simplicity is required for power system stability analysis. To accomplish this goal, an accurate aggregated modified sequence impedance model of the wind farm is established in this paper. The modified sequence impedance model of wind turbine generator is established, which considers the coupling between the positive- and negative-sequence impedances. The modified sequence impedances of the ac collection system, transformers, and ac grid are also derived. In this way, the impedance network of the entire wind farm system can be formed and simplified to acquire the accurate aggregated modified sequence impedance. Furthermore, the proposed model is compared with the traditional single-machine aggregated model which shows the necessity of establishing the accurate aggregated model. It is worth noting that the differences among each wind turbine generator's operation points can be included in the proposed model. Compared with the results of impedance measurements of a target wind farm, the accuracy of the proposed aggregated sequence impedance model of the wind farm is verified in frequency domain. The application of the proposed model in the stability analysis of a grid-connected wind farm is also presented with consideration of the ac grid strength. What is more, the effect of the inertial controller on the wind farm system stability is also analyzed to make the impact of this study much more appealing and up to date.

Nomenclature

C_W	Capacitance of dc bus capacitor
f_0	Grid frequency
f_s	Switching frequency
I_{wdq0}	PCC current steady-state value
I_{dcw}	WTG dc bus current
i_{wdq}	*d*- and *q*-axis components of WTG current
k_{pPLL}	Proportional gain of PLL
k_{iPLL}	Integral gain of PLL
k_{pi}	Proportional gain of current loop
k_{ii}	Integral gain of current controller
k_{pu}	Proportional gain of voltage loop
k_{iu}	Integral gain of voltage loop
$k_{inertia}$	Proportional gain of the inertia controller
L_W	Inductance of WTG inductor
L_L	Inductance of 35 kV bus
P_W	WTG rated active power
Q_W	WTG rated reactive power
R_W*Resistance of WTG resistor*R_L	Resistance of 35 kV bus
SISO	Single-input-single-output
SCR	Short circuit ratio
U_g	RMS value of the grid voltage
U_{wdq0}	PCC voltage steady-state value
U_{dcw}	WTG dc bus voltage
u_{wdq}	*d*- and *q*-axis components of WTG voltage
V_{wdq_ref0}	Modulation voltage steady-state value
ν_{wdq_ref}	*d*- and *q*-axis components of modulation voltage
WTG	wind turbine generator
$\boldsymbol{Z}_{wdq}$	WTG *d*-*q* impedance
$\boldsymbol{Z}_{wpn}$	WTG modified sequence impedance
$\boldsymbol{Z}_T$	Transformer modified sequence impedance
$\boldsymbol{Z}_L$	Cable modified sequence impedance
Z_{pn}^{WF}	Wind farm SISO sequence impedance
Z_{pn}^{G}	Grid system SISO sequence impedance

* Corresponding author at: Wind Power Research Centre (WPRC), Shanghai Jiao Tong University (SJTU), No. 800 Dongchuan Road, Shanghai, China.
Email address: xucai@sjtu.edu.cn (X. Cai)

https://doi.org/10.1016/j.epsr.2019.105928
Received 23 October 2018; Received in revised form 30 April 2019; Accepted 21 June 2019
Available online xxx
0378-7796/

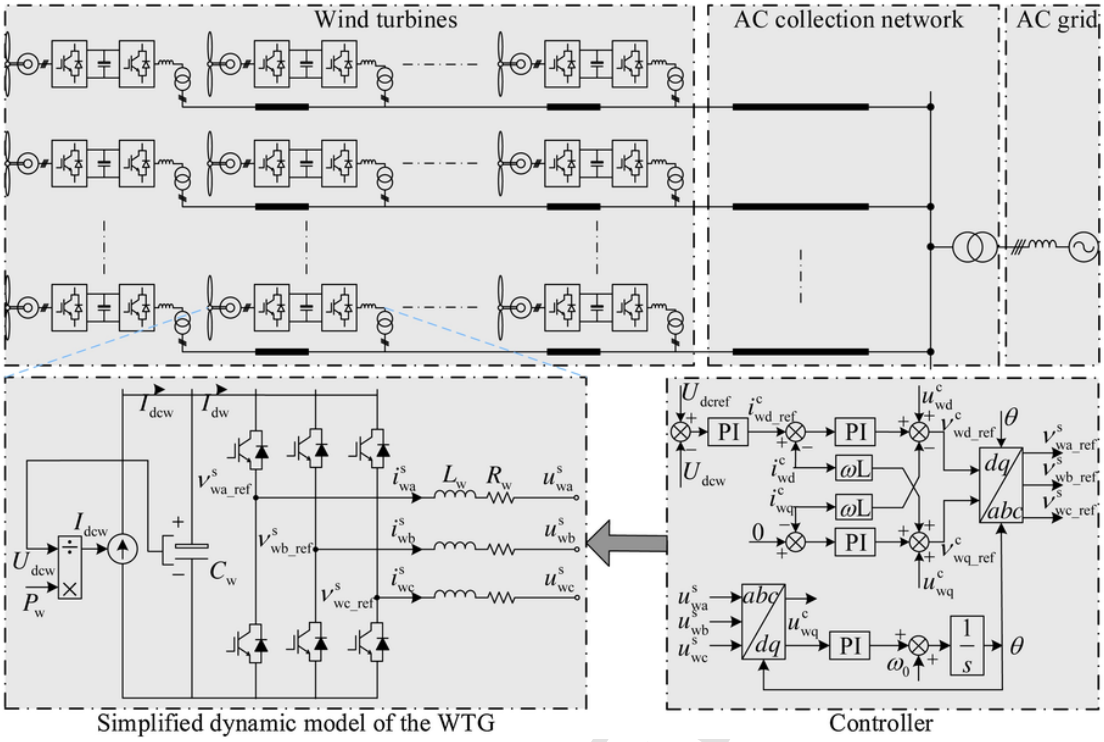

Fig. 1. General topology of the studied wind farm.

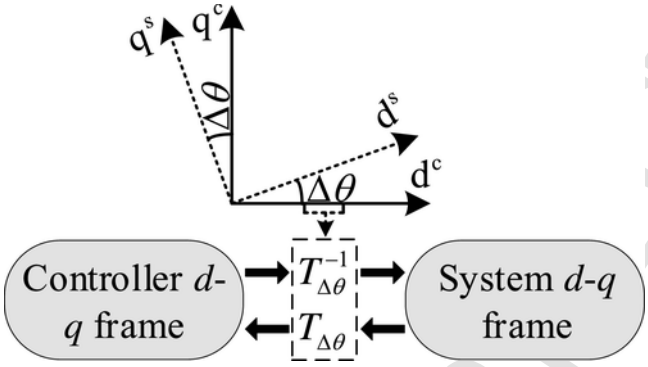

Fig. 2. Relationship between the controller *d-q* frame and the system *d-q* frame.

1. Introduction

With the fast consumption of fossil fuels and the deterioration of the environment, wind power is taking a more prominent role in power generation. 51.3 GW of new wind power capacity was installed in 2018, bringing total installations to 591 GW globally [1]. However, due to the high penetration level of the wind power, grid-connected wind farms have begun to significantly affect the power system dynamics resulting in stability issues [2], such as oscillation/resonance phenomena. What is more, since power system operators set technical requirements for wind farms to provide the frequency support in the future [3,4], the interaction between wind farms and the grid will become much more complicated. Therefore, it is a necessity to study the wind farms' dynamics as well as their effects on the power system stability. To accomplish the above research, the first step is to establish a suitable wind farm model taking both accuracy and simplicity into account.

Currently, there are mainly two kinds of approaches to analyze the small-signal stability of grid-connected wind farm, i.e. eigen value-based method and impedance-based method. In terms of the eigenvalue-based method, the state-space model of the wind farm is established and then analyzed by classical eigenvalue analysis method. Generally, a wind farm can be represented and modeled in detailed manners [5], or in aggregated manners including single-machine aggregated model [6,7], semi-aggregation model [8,9] and multi-machine aggregated model [10]. In all these models, the wind farm is represented with one high-order linearized state-space model. The disadvantage with these approaches is that the model is bulky, as the entire system must be modelled as a single state-space representation, which must be rebuilt in case of variation in the network topology or components. Furthermore, Ref. [11] shows that using aggregated wind farm

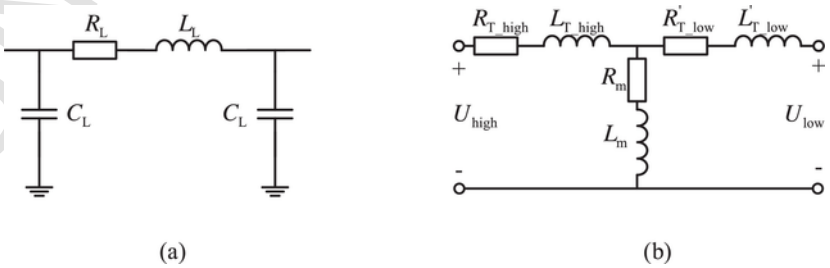

Fig. 3. Impedance model of passive components. (a) Cable. (b) Transformer.

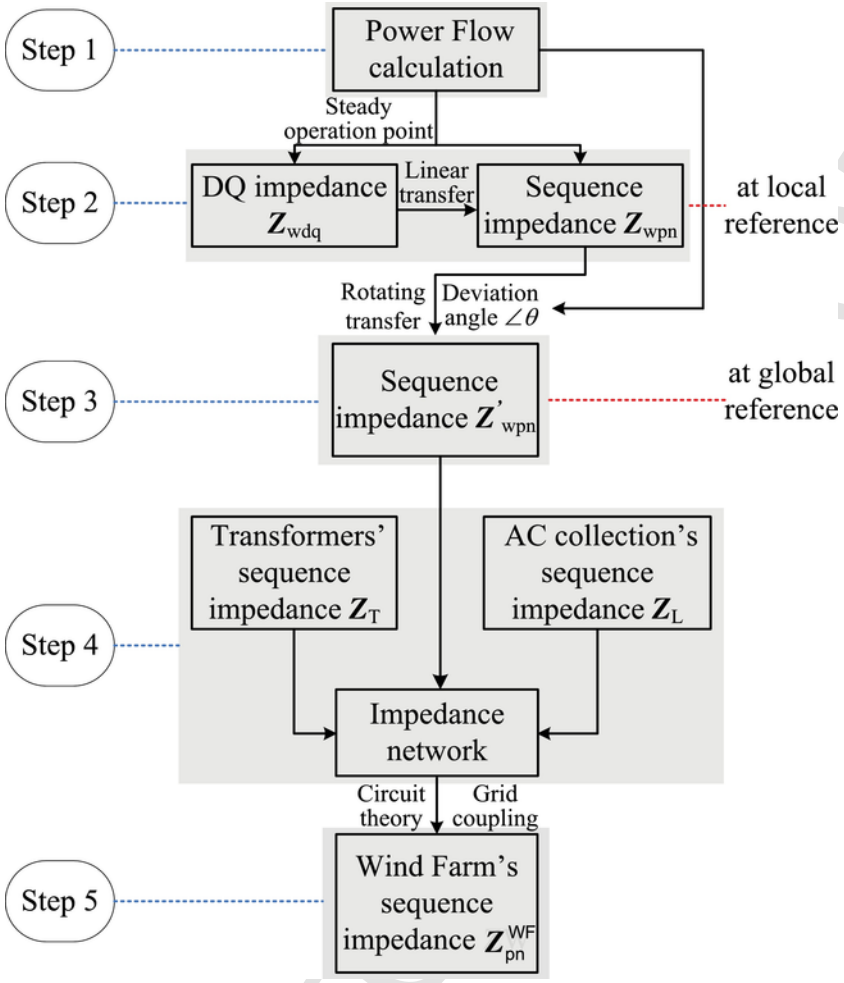

Fig. 4. Procedure for obtaining the accurate aggregation of sequence impedance of the wind farm.

system is difficult to accurately judge the system stability due to the possibility of losing some internal resonant modes or changing their characteristics during the aggregation process. The literature [12] made contributions in equivalencing the collector system of a large wind farm based on the energy conservation law. Ref. [13] validated the equivalent model of wind farm [12] in steady and transient state. However, they both neglected most of converters' dynamics which are not suitable for today's converter-based grid-connected wind farm system.

Another approach is the impedance-based method which has been widely applied in the stability analysis of the power electronic systems. Compared to the eigenvalue-based method, the impedance theory has formidable advantages in the stability analysis of large power systems, such as modularity, simplicity and convenience. The essence of the impedance-based stability criterion, first presented in Ref. [14], is to divide the studied system into a source subsystem and a load subsystem for system-level analysis. Previous works have derived models of, e.g., three-phase voltage source converters (VSC) [15,16], modular multilevel converters [17], and so on. Three main types of impedance domains have been established, i.e., sequence domain [15], *d-q* domain [16] and modified sequence domain [18–20]. Relationships among these three domains are also well established in the literature [21–23]. Ref. [15] proposed a simplified sequence impedance which assumes that positive- and negative-sequence impedances are decoupled, and the grid is ideal. Considering the asymmetric conditions and coupling between *d* axis and *q* axis, one version of accurate impedance modelling called *d-q* impedance is proposed [16,24]. Recently, Rygg et. al. proposed a modified sequence impedance concept [18], and found the equivalence relation between the *d-q* impedance and the modified sequence impedance concept [23]. Based on this, the single-input-single-output (SISO) equivalent sequence model was proposed by Zhang et al. [25] and the corresponding stability criterion was also established. The advantages of the modified sequence domain over the *d-q* domain and original sequence domain have been discussed well in Ref. [16], such as accuracy of the stability analysis, convenience of practical measurement, time invariant characteristic and more intuitive interpretation of physical meaning.

In terms of the grid-connected wind farm stability analysis, few researches use the impedance-based method to model the wind farm. Ref. [26] analyzed the effect of the number of DFIG upon the wind farm's impedance characteristics via the frequency scanning. Refs. [27,28] modeled the wind farm via single-machine aggregated model, which simplify the wind farm a lot. Ref. [29] still modeled the DFIG-based wind farm via single-machine aggregated model and the correctness of multiple wind farms' aggregated *d-q* impedance is not verified by simulations. So far, most literatures use the single-machine aggregated model of the wind farm which neglects impedance couplings and the accuracy is not verified. Also, due to the requirement for the wind farm to provide the frequency support, it is necessary to analyze the wind power frequency control's effects on the power system stability, which has not been attached with enough importance [30,31]. In this paper, the accurate aggregated modified sequence impedance modelling method for wind farm systems is presented, by which all components of the wind farm can be properly considered including each

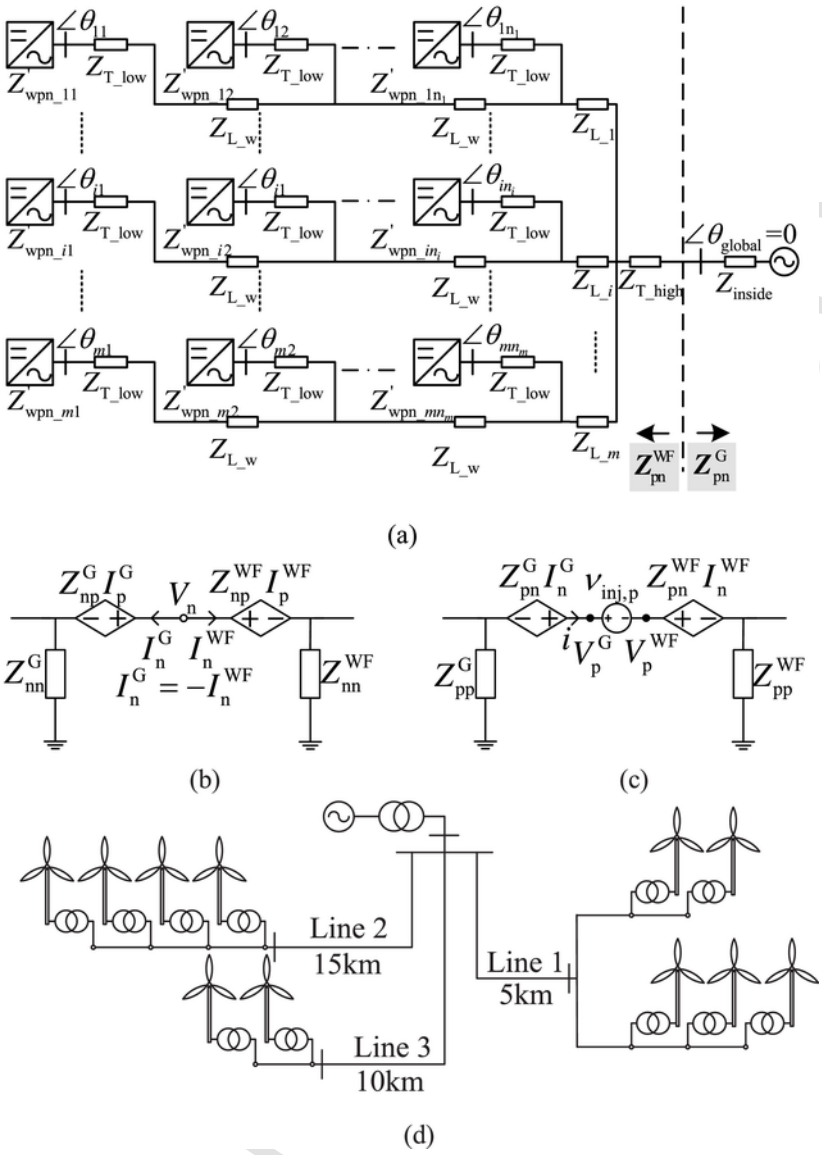

Fig. 5. Impedance network and topology of the studied wind farm. (a) Impedance network. (b) Positive sequence equivalent circuit. (c) Negative sequence equivalent circuit. (d) Topology of the studied wind farm.

WTG's dynamics, transformers' dynamics and the ac collection network characteristics. Compared with the high-order state-space wind farm model, the proposed method is modular, thus flexible to the variation in the network topology and components. The proposed model can reflect the difference of WTGs' operation points without adding up the amount of calculation. The off-diagonal sequence coupling is taken into account in the proposed sequence model. Compared with the traditional single-machine aggregated model, the proposed model is more accurate in frequency domain. Based on such model, the inertial controller's impacts on the power system stability is analyzed which has negative influences on the stability margin.

The rest of this paper is organized as follows. In Section 2, the accurate modified sequence impedance model of the wind farm is established. In Section 3, the procedure of the aggregation modelling is expounded. In Section 4, a target wind farm consisting of 11 wind turbines is built in Matlab/Simulink to validate the correctness of the proposed model. In Section 5, the application of such model to the stability analysis of the grid connected wind farm is demonstrated. The time-domain simulation results validate the theoretical analysis. In Section 6, each WTG is attached with the inertial controller whose impacts on the system stability are discussed.

2. Accurate modified sequence impedance modelling of wind farm components

2.1. System description

The general topology of the studied wind farm is depicted in Fig. 1, where the WTG is based on permanent magnetic direct drive wind turbine (PMSG) and hundreds of WTGs are interconnected via the AC collection network. The AC grid is equivalent to an ideal voltage source in series with an impedance which can be used to regulate the grid strength, i.e. short circuit ratio (SCR). For simplification of analysis, the turbine mechanical system and machine side converter are replaced with a constant power load (CPL), since the machine side dynamics have less impact on the grid side dynamics [32]. According to Ref. [33], it's rational to simplify the PMSG as a CPL-based model in stability analysis of a large wind farm system, because the CPL-based model

Table 1
Electrical parameters of the target wind farm.

Parameters	Symbol	Value	Parameters	Symbol	Value
Grid voltage	U_g	110 kV	PLL proportional gain	k_{pPLL}	120
Grid Frequency	f_0	50 Hz	PLL integral gain	k_{iPLL}	2800
DC bus voltage	U_{dc}	1100 V	Current loop proportional gain	k_{pi}	0.15
WTG rated active power	P_W	2 MW	Current loop integral gain	k_{ii}	10.72
WTG rated reactive power	Q_W	0 kVar	Voltage loop proportional gain	k_{pu}	2
Switching frequency	f_s	2 kHz	Voltage loop integral gain	k_{iu}	25
Short circuit ratio	SCR	10	DC bus capacitor	C_W	35 mF
WTG filter inductance	L_W	0.15 mH	35 kV-bus resistance	R_L	0.18 Ω/km
Inertia control gain	$k_{inertia}$	50 p.u.	35 kV-bus inductance	L_L	1.2 mH/km

Table 2
Parameters of transformers.

	Description	Value
0.69 kV/35 kV transformer	Rated capacity	2 MVA
	Primary side [R1,L1]	[0.016,0.06] pu
	Secondary side [R2,L2]	[0.016,0.06] pu
35 kV/110 kV transformer	Rated capacity	25 MVA
	Primary side [R1,L1]	[0.0125,0.1] pu
	Secondary side [R2,L2]	[0.0125,0.1] pu

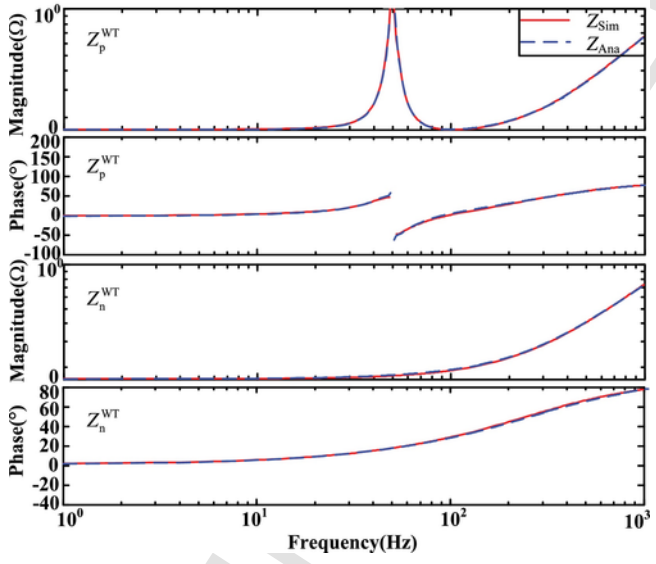

Fig. 6. Impedance model verification of the single WTG connected to the ideal grid.

of the PMSG-based WTG is pessimistic for the stability margin. The simplified WTG and its controller are also shown in Fig. 1.

A small advantage with the *d-q* domain impedance model is that the analytical models are normally easier to derive than in other domains. It's better to derive models in the *d-q* domain, and then transform them into the modified sequence domain when performing the stability analysis. Therefore, in this section, the *d-q* impedance model of the single WTG is first derived, and then is transformed into the modified sequence domain via a linear transformation [18]. Besides, modified sequence impedances of other components in the wind farm are also given.

2.2. D-Q impedance modelling of WTG

Assuming that systems are linear time invariant (LTI) in the *d-q* domain has been commonly applied in the impedance modeling and is often a good approximation [18]. Strong nonlinearities like saturation are not considered in this paper. Due to the effect of the PLL, two *d-q* frames exist in the converter system, i.e., the system *d-q* frame and controller *d-q* frame [16]. The controller *d-q* frame is defined by the PLL, which tracks the angle and frequency of the grid voltage to synchronize with the system *d-q* frame. In a steady state, the controller *d-q* frame is aligned with the system *d-q* frame, whereas the deviation occurs when small signal perturbations are injected into to the grid voltage or current. The relationship between these two *d-q* frames is shown in Fig. 2 and the transfer matrix $\boldsymbol{T}_{\Delta\theta}$ is given in Eq. (1).

$$\boldsymbol{T}_{\Delta\theta} = \begin{bmatrix} \cos\Delta\theta & \sin\Delta\theta \\ -\sin\Delta\theta & \cos\Delta\theta \end{bmatrix} \tag{1}$$

where $\Delta\theta$ is the deviation angle between the controller *d-q* frame and the system *d-q* frame.

The state-space model of a three-phase voltage source converter in the *d-q* frame is given in Eqs. (2) and (3).

$$\frac{\mathrm{d}}{\mathrm{d}t}\begin{bmatrix} i^{s}_{wd} \\ i^{s}_{wq} \\ U_{dcw} \end{bmatrix} = \begin{bmatrix} \frac{-R_w}{L_w} & \omega_0 & \frac{v^{s}_{wd\_ref}}{L_w U_{dcw0}} \\ -\omega_0 & \frac{-R_w}{L_w} & \frac{v^{s}_{wq\_ref}}{L_w U_{dcw0}} \\ \frac{-v^{s}_{wd\_ref}}{C_w U_{dcw0}} & \frac{-v^{s}_{wq\_ref}}{C_w U_{dcw0}} & 0 \end{bmatrix} \cdot \begin{bmatrix} i^{s}_{wd} \\ i^{s}_{wq} \\ U_{dcw} \end{bmatrix} - \begin{bmatrix} 1/L_w & 0 & 0 \\ 0 & 1/L_w & 0 \\ 0 & 0 & -1/C_w \end{bmatrix} \cdot \begin{bmatrix} u^{s}_{wd} \\ u^{s}_{wq} \\ I_{dcw} \end{bmatrix} \tag{2}$$

$$\begin{aligned} v^{c}_{wd\_ref} &= (k_{pi} + \frac{k_{ii}}{s}) \cdot (i^{c}_{wd\_ref} - i^{c}_{wd}) - i^{c}_{wq} \cdot \omega_0 L + u^{c}_{wd} \\ v^{c}_{wq\_ref} &= (k_{pi} + \frac{k_{ii}}{s}) \cdot (i^{c}_{wq\_ref} - i^{c}_{wq}) + i^{c}_{wd} \cdot \omega_0 L + u^{c}_{wq} \\ i^{c}_{wd\_ref} &= (k_{pu} + \frac{k_{iu}}{s}) \cdot (U_{dcref} - U_{dcw}) \\ \theta &= \frac{1}{s} \cdot [\omega_0 - (k_{pPLL} + \frac{k_{iPLL}}{s}) \cdot u^{c}_{wq}] \end{aligned} \tag{3}$$

where the superscript s represents the system *d-q* frame and the superscript c represents the controller *d-q* frame.

By applying linearization and Laplace transformation to Eqs. (2) and (3), the linearized equations in *s* domain can be obtained as Eqs. (4) and (5).

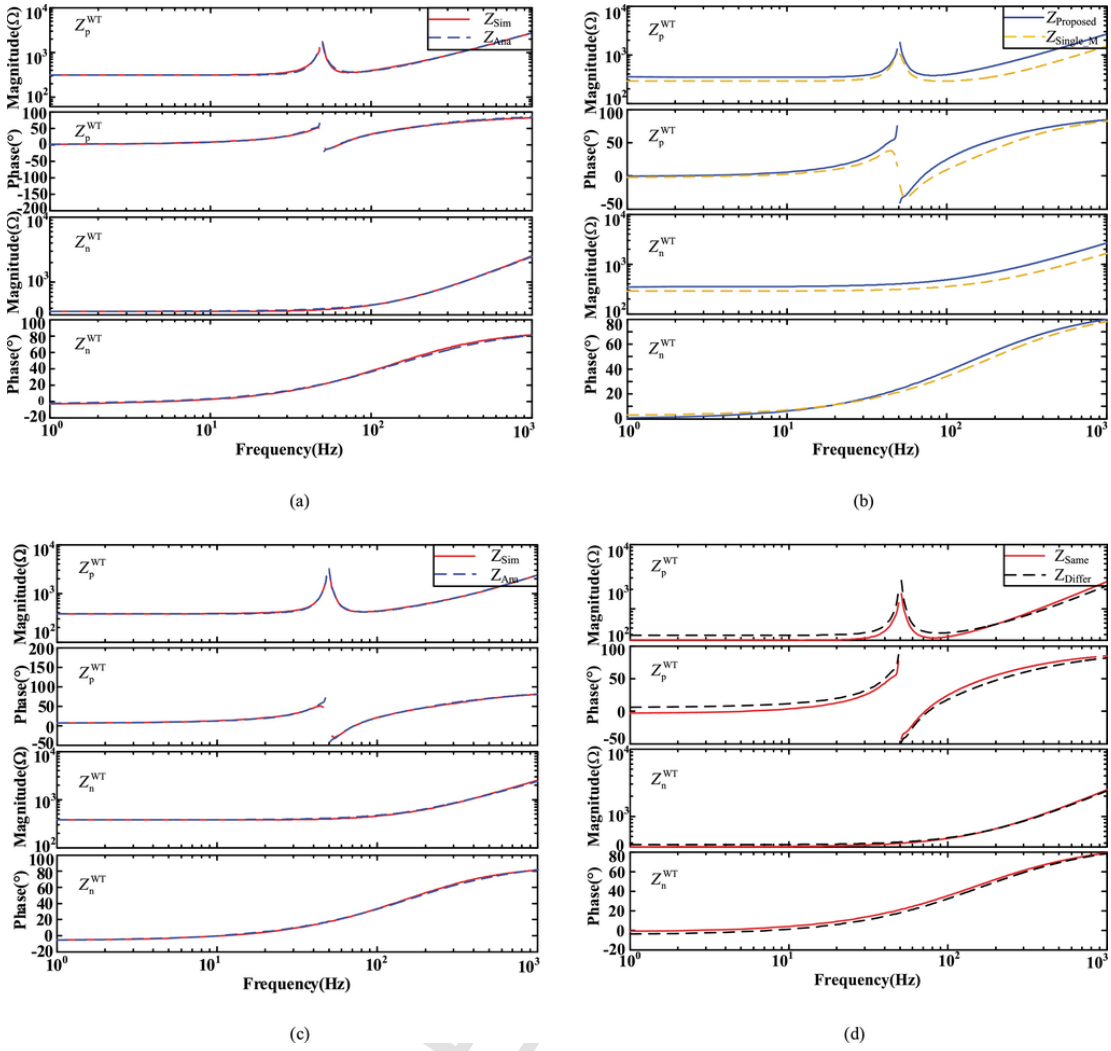

Fig. 7. Validation of the proposed accurate aggregated sequence impedance model for the wind farm. (a) Proposed model verification of the wind farm when all WTGs receive same wind speed. (b) Comparison between the impedances obtained by the proposed model and the single-machine model. (c) Proposed model verification of the wind farm when WTGs receive different wind speeds. (d) Impact of wind speed distribution on the wind farm impedance characteristics.

$$
s\begin{bmatrix}\Delta i^{s}_{wd}\\ \Delta i^{s}_{wq}\\ \Delta U_{dcw}\end{bmatrix}=\begin{bmatrix}\frac{-R_w}{L_w} & \omega_0 & \frac{V_{wd\_ref0}}{L_w U_{dcw0}}\\ -\omega_0 & \frac{-R_w}{L_w} & \frac{V_{wq\_ref0}}{L_w U_{dcw0}}\\ \frac{-V_{wd\_ref0}}{C_w U_{dcw0}} & \frac{-V_{wq\_ref0}}{C_w U_{dcw0}} & 0\end{bmatrix}\cdot\begin{bmatrix}\Delta i^{s}_{wd}\\ \Delta i^{s}_{wq}\\ \Delta U_{dcw}\end{bmatrix}-\begin{bmatrix}\frac{1}{L_w} & 0 & 0\\ 0 & \frac{1}{L_w} & 0\\ 0 & 0 & \frac{-1}{C_w}\end{bmatrix}\cdot\begin{bmatrix}\Delta u^{s}_{wd}\\ \Delta u^{s}_{wq}\\ 0\end{bmatrix}+\begin{bmatrix}\frac{1}{L_w} & 0\\ 0 & \frac{1}{L_w}\\ \frac{-I_{wd0}}{C_w U_{dcw0}} & \frac{-I_{wq0}}{C_w U_{dcw0}}\end{bmatrix}\cdot\begin{bmatrix}\Delta v^{s}_{wd\_ref}\\ \Delta v^{s}_{wq\_ref}\end{bmatrix} \tag{4}
$$

$$
\begin{aligned}
\Delta i^{c}_{wd\_ref} &= -(k_{pu}+\frac{k_{iu}}{s})\cdot\Delta U_{dcw}\\
\Delta v^{c}_{wd\_ref} &= (k_{pi}+\frac{k_{ii}}{s})\cdot(\Delta i^{c}_{wd\_ref}-\Delta i^{c}_{wd})-\Delta i^{c}_{wq}\cdot\omega_0 L_W+\Delta u^{c}_{wd}\\
\Delta v^{c}_{wq\_ref} &= (k_{pi}+\frac{k_{ii}}{s})\cdot(\Delta i^{c}_{wq\_ref}-\Delta i^{c}_{wq})+\Delta i^{c}_{wd}\cdot\omega_0 L_W+\Delta u^{c}_{wq}\\
\Delta\theta &= -\frac{1}{s}\cdot(k_{pPLL}+\frac{k_{iPLL}}{s})\cdot\Delta u^{c}_{wq}
\end{aligned} \tag{5}
$$

where the subscript 0 denotes the steady state value of state variables. Additionally, the relations between variables at the system *d-q* frame and controller *d-q* frame are shown in Eq. (6). The detailed derivation process can be referred to Ref. [34].

$$
\begin{aligned}
\Delta u^{s}_{wd} &= \Delta u^{c}_{wd}-\Delta\theta\cdot U_{wq0}\\
\Delta u^{s}_{wq} &= \Delta u^{c}_{wq}+\Delta\theta\cdot U_{wd0}\\
\Delta i^{s}_{wd} &= \Delta i^{c}_{wd}-\Delta\theta\cdot I_{wq0}\\
\Delta i^{s}_{wq} &= \Delta i^{c}_{wq}+\Delta\theta\cdot I_{wd0}\\
\Delta v^{s}_{wd\_ref} &= \Delta v^{c}_{wd\_ref}-\Delta\theta\cdot V_{wq\_ref0}\\
\Delta v^{s}_{wq\_ref} &= \Delta v^{c}_{wq\_ref}-\Delta\theta\cdot V_{wd\_ref0}
\end{aligned} \tag{6}
$$

Taking $\Delta\boldsymbol{i}$s wdq as input variable and $\Delta\boldsymbol{u}$s wdq as output variable, Eqs. (4)–(6) can be expressed in the state space form like Eq. (7).

$$
\begin{aligned}
s\Delta\boldsymbol{x} &= \boldsymbol{A}\Delta\boldsymbol{x}+\boldsymbol{B}\Delta\boldsymbol{i}^{s}_{wdq}\\
\Delta\boldsymbol{u}^{s}_{wdq} &= \boldsymbol{C}\Delta\boldsymbol{x}+\boldsymbol{D}\Delta\boldsymbol{i}^{s}_{wdq}
\end{aligned} \tag{7}
$$

where $\boldsymbol{x}$ are state vectors, Δ denotes the deviation operation, the definition of $\boldsymbol{A}$, $\boldsymbol{B}$, $\boldsymbol{C}$, $\boldsymbol{D}$ is listed in Appendix C.

Hence, the transfer function relationship between $\Delta\boldsymbol{u}$s wdq and $\Delta\boldsymbol{i}$s wdq can be established based on Eq. (7). As a result, the *d-q* impedance $\boldsymbol{Z}_{wdq}$ of the WTG can be obtained by the ratio of the output $\Delta\boldsymbol{u}$s wdq to

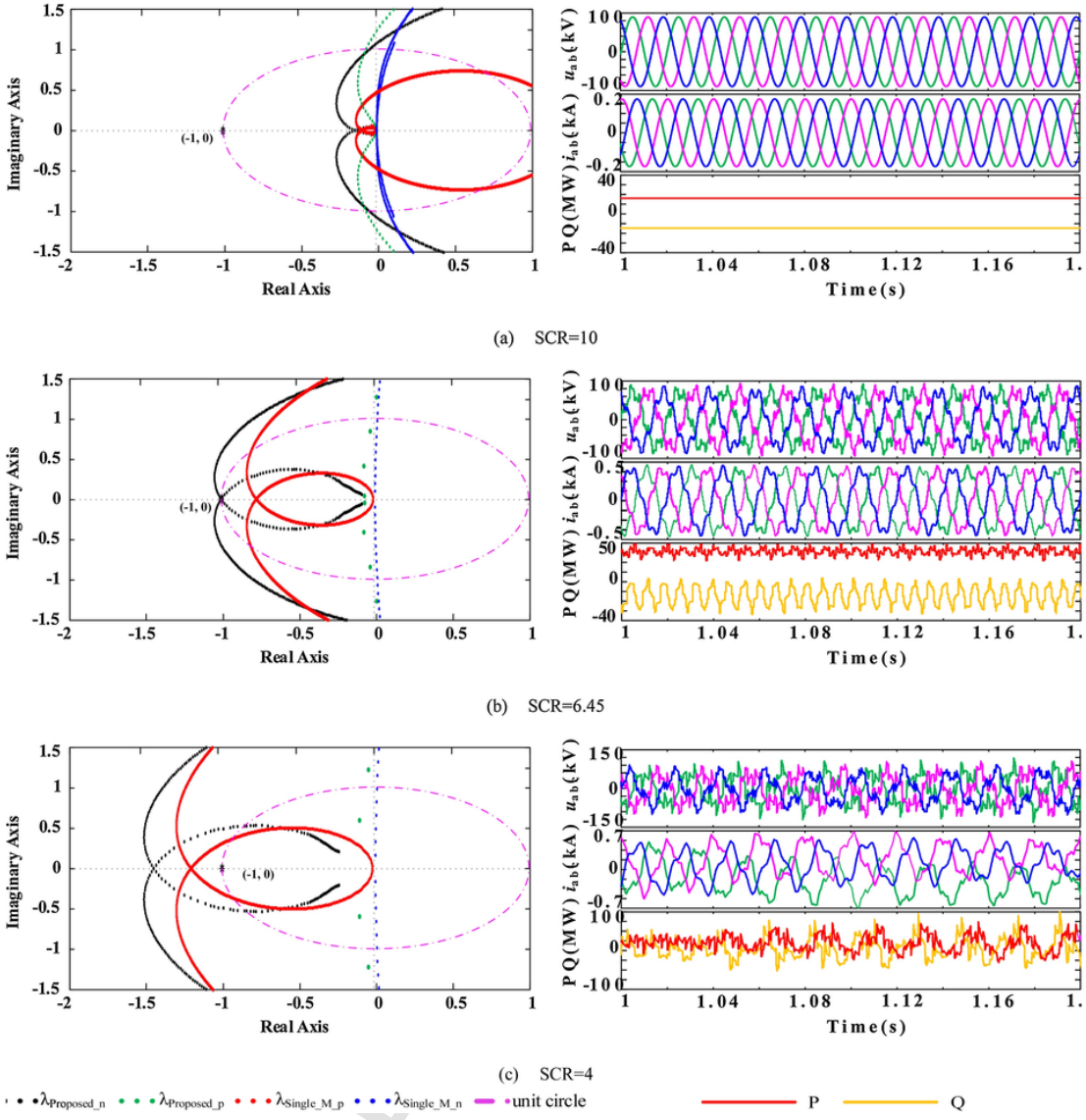

Fig. 8. Comparison of the root locus of L_{pn} between the proposed model and the single-machine aggregated model under different SCR, and the proposed model's corresponding simulation waveforms. (a) SCR = 10. (b) SCR = 6.45. (c) SCR = 4.

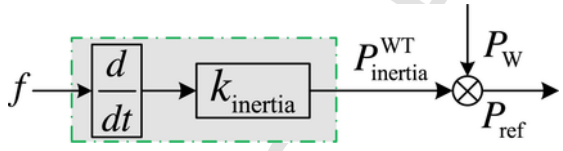

Fig. 9. Inertial controller.

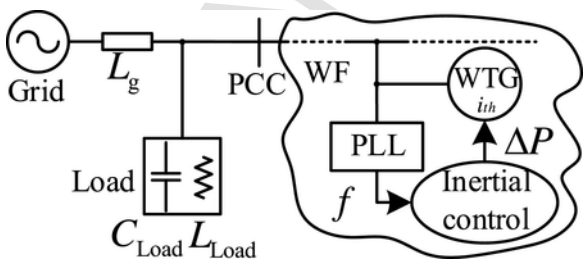

Fig. 10. Grid-connected wind farm with local load.

the input $\Delta \boldsymbol{i}$s wdq, which is generally expressed as Eq. (8).

$$\begin{bmatrix}\Delta u^{s}_{wd}\\ \Delta u^{s}_{wq}\end{bmatrix}=\begin{bmatrix}Z_{wdd} & Z_{wdq}\\ Z_{wqd} & Z_{wqq}\end{bmatrix}\cdot\begin{bmatrix}\Delta i^{s}_{wd}\\ \Delta i^{s}_{wq}\end{bmatrix}=\boldsymbol{Z}_{wdq}\cdot\begin{bmatrix}\Delta i^{s}_{wd}\\ \Delta i^{s}_{wq}\end{bmatrix} \tag{8}$$

2.3. Modified sequence impedance modelling of WTG

The sequence domain is widely applied in power system analysis for its capability to decompose unbalanced three-phase systems into three balanced and decoupled subsystems, i.e., positive sequence subsystem (*p*), negative sequence subsystem (*n*), and zero sequence subsystem (0). It's more convenient and intuitive to analyze the system stability via sequence impedance rather than *d*-*q* impedance. Before deriving the sequence domain model, the modified sequence domain model needs to be derived which connects the *d*-*q* domain with the sequence domain. In this section, the *d*-*q* impedance of the WTG derived in Section 2.1 will be transformed into modified sequence impedance based on a linearization method presented in Ref. [18].

The 0-axis can be dropped for balanced three-phase systems or systems without neutral connection (hence no 0-axis current can flow).

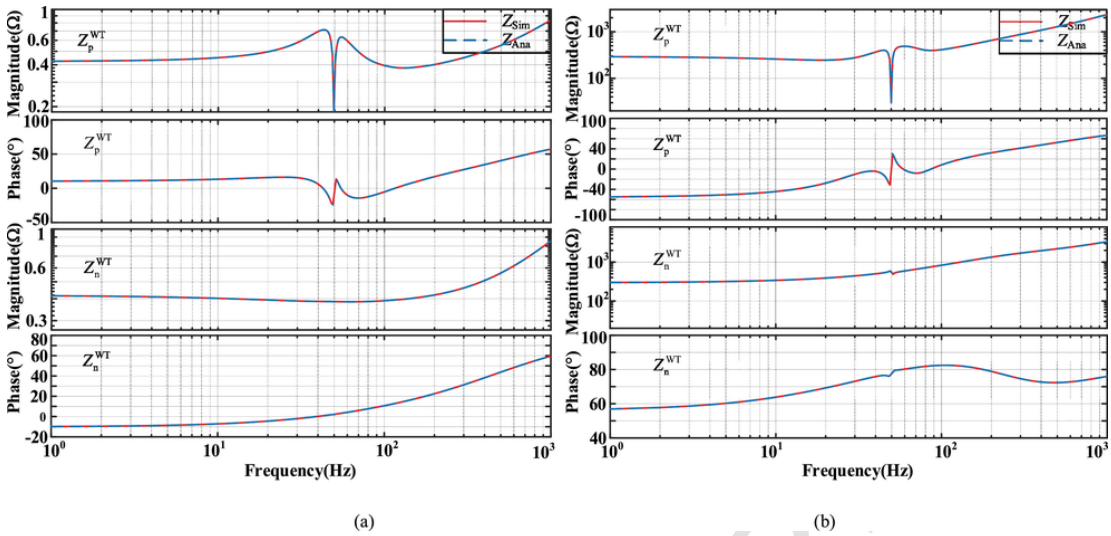

Fig. 11. Impedance model verification with the inertia controller. (a) Single machine; (b) Wind farm ($k_{inertial}$ = 50 p.u).

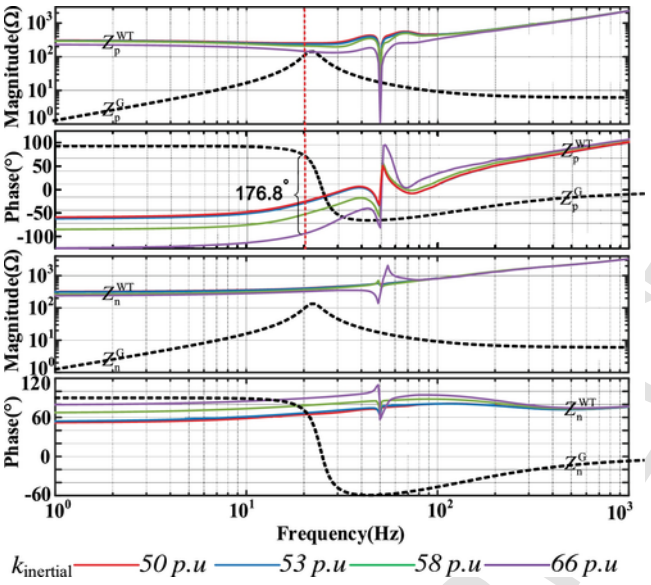

Fig. 12. Effects of the inertial controller on the system stability.

Similar to the grid-connected system in Refs. [15,16,18], there exists no 0-axis component in this paper's model because of no neutral connection and steady-state operation. Therefore, the 0-axis is disregarded in both park and sequence transformation. The relationship between the *abc* coordinate frame and *d-q* coordinate frame can be expressed as.

$$\begin{bmatrix} v_d \\ v_q \end{bmatrix} = \sqrt{\frac{2}{3}} \cdot \begin{bmatrix} \cos\alpha & \cos(\alpha - \frac{2\pi}{3}) & \cos(\alpha + \frac{2\pi}{3}) \\ -\sin\alpha & -\sin(\alpha - \frac{2\pi}{3}) & -\sin(\alpha + \frac{2\pi}{3}) \end{bmatrix} \cdot \begin{bmatrix} v_a \\ v_b \\ v_c \end{bmatrix} \tag{9}$$

The relationship between a time-domain waveform and its frequency-domain components is

$$v(t) = \sum_{k=0}^{\infty} v_k \cos\left(\omega_k + \theta_k\right) \tag{10}$$

$$V_k = v_k e^{j\theta_k} \tag{11}$$

The *abc* phasors can be related to sequence domain phasors by the symmetric component transform in Eq. (12).

$$\begin{bmatrix} V_p \\ V_n \end{bmatrix} = \begin{bmatrix} 1 & a & a^2 \\ 1 & a^2 & a \end{bmatrix} \cdot \begin{bmatrix} v_a \\ v_b \\ v_c \end{bmatrix} \tag{12}$$

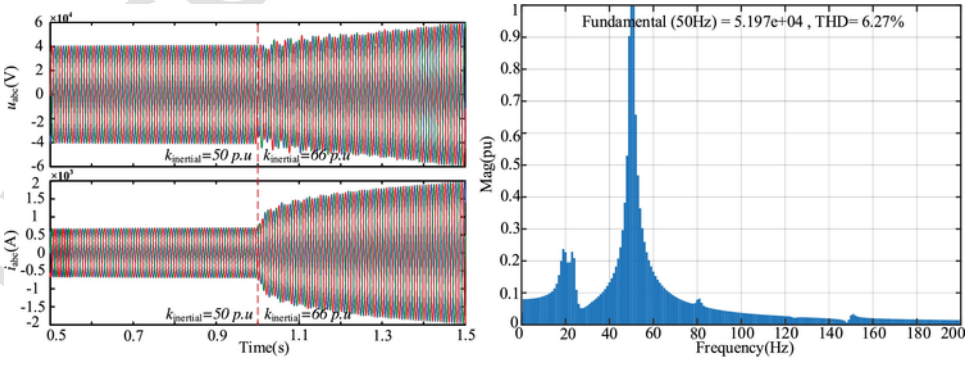

Fig. 13. Verifications of the stability analysis. (a) PCC voltage and current (0.5 s~1.5 s); (b) frequency spectrogram of the PCC current (t > 1 s).

Table B1
Electrical parameters of the target wind farm.

WTG	U_{gd} (V)	U_{gq} (V)	I_{gd} (A)	I_{gq} (A)	Angle (°)	P (MW)
1	486	−222	2755	0	66.7	2
2	488	−220	2730	0	66.6	2
3	480	−229	2800	0	67.0	2
4	482	−228	2757	0	66.9	2
5	485	−223	2735	0	66.7	2
6	444	−273	2998	0	68.5	2
7	447	−270	2976	0	68.4	2
8	452	−264	2944	0	68.1	2
9	458	−253	2900	0	67.7	2
10	509	−155	2615	0	63.5	2
11	529	−141	2514	0	63.4	2

Table B2
Electrical parameters of the target wind farm.

WTG	U_{gd} (V)	U_{gq} (V)	I_{gd} (A)	I_{gq} (A)	Angle(°)	P (MW)
1	490	−225	2581	0	65.7	1.9
2	492	−222	2567	0	65.6	1.9
3	485	−234	2468	0	66.0	1.8
4	487	−231	2458	0	65.9	1.8
5	490	−225	2441	0	65.7	1.8
6	455	−280	2043	0	65.9	1.4
7	458	−276	2032	0	65.8	1.4
8	462	−270	2011	0	65.6	1.4
9	469	−260	1983	0	65.4	1.4
10	533	−145	1248	0	62.3	1
11	534	−142	1246	0	62.3	1

Based on the above relationship among the *abc* frame, *d-q* frame, and sequence domain, the relationship between the *d-q* impedance and modified sequence impedance can be obtained as Eq. (13). The detailed derivation can be found in Appendix D [18]. Hence, the WTG's modified sequence impedance can be obtained by applying the transformation in Eq. (13) to the *d-q* impedance in Eq. (8). It is noted that the impedance $\boldsymbol{Z}_{\text{wpn}}$ in Eq. (14) is a 2×2 matrix which is defined as the modified sequence impedance [23]. This paper is focused on small-signal stability analysis of the wind farm. Therefore, the time domain changes of the sequence domain are disregarded. It is worth noting that in most applications of the sequence domain, only the fundamental frequency components are considered. However, in modified sequence domain, positive and negative sequences are defined at two different frequencies, shifted by twice the fundamental frequency, which means the phasors can be related to any frequency [18].

$$\begin{gathered}\boldsymbol{Z}_{\text{wpn}} = \boldsymbol{A}_Z \cdot \boldsymbol{Z}_{\text{wdq}} \cdot \boldsymbol{A}_Z^{-1} \\ \boldsymbol{A}_Z = \frac{1}{\sqrt{2}}\begin{bmatrix} 1 & j \\ 1 & -j \end{bmatrix}, \boldsymbol{A}_Z^{-1} = \frac{1}{\sqrt{2}}\begin{bmatrix} 1 & 1 \\ -j & j \end{bmatrix}\end{gathered} \tag{13}$$

where

$$\boldsymbol{Z}_{\text{wpn}} = \begin{bmatrix} Z_{\text{wpp}} & Z_{\text{wpn}} \\ Z_{\text{wnp}} & Z_{\text{wnn}} \end{bmatrix} \tag{14}$$

2.4. Modified sequence impedances of cable and transformer

For cables in the wind farm, the lumped-parameter π-type equivalent circuit model is used as shown in Fig. 3(a), where *R*, *L*, *C* are lumped resistance, inductance and shunt capacitance respectively. Generally, the shunt capacitance has very little effect on the SSR characteristics and thus can be neglected. For transformers in the wind farm, the T-type equivalent circuit model is applied as shown in Fig. 3(b). In the excitation branch, R_{m} and L_{m} represent the excitation resistance and inductance respectively, which is large enough to be approximate to the open circuit. $R_{\text{T\_high}}$ and $L_{\text{T\_high}}$ are the primary resistance and inductance respectively, while *R*' T_low and *L*' T_low are the secondary resistance and inductance respectively which have been converted into the high voltage side.

Since the cable and the transformer are all passive components, there is no coupling between the positive- and negative-sequence impedances. Based on Fig. 3, the sequence impedances of the transformer and cable can be expressed in Eqs. (15) and (16), respectively.

$$\boldsymbol{Z}_{\text{T}} = (R_{\text{T\_high}} + R'_{\text{T\_low}})\boldsymbol{I} + s \cdot (L_{\text{T\_high}} + L'_{\text{T\_low}})\boldsymbol{I} \tag{15}$$

$$\boldsymbol{Z}_{\text{L}} = (R_{\text{L}} + sL_{\text{L}})\boldsymbol{I} \tag{16}$$

where $\boldsymbol{I}$ is 2×2 unit matrix.

3. The accurate aggregated modified sequence impedance modelling of wind farm systems

The modified sequence impedances of WTG, cable, and transformer have been derived in the previous section, which is the basis of the wind farm modified sequence impedance modelling. In this section, the accurate aggregated modified sequence impedance modelling of wind farm system is presented. The modelling procedure of the accurate aggregated modified sequence impedance model of the wind farm is shown in Fig. 4, which is expounded as follows. Although the PMSG-based wind farm is used as a case study in this paper, the concept of this aggregation procedure is applicable to other types of wind farms. It's only left to replace the impedance model of the PMSG with other types of WTG.

1) The power flow calculation is performed to obtain the steady state operating point.
2) The *d-q* impedance of each WTG is calculated and then transformed into the modified sequence impedance at its local reference frame.
3) The modified sequence impedance of the WTG at the local reference frame is then converted into global Ref. [35].
4) The modified sequence impedances of the transformers and cables need to be provided, which forms the whole impedance network of the wind farm together with the WTG impedances.
5) Based on standard circuit theory, the accurate aggregated modified impedance of the wind farm can be obtained.

In analogy to the relationship between the controller *d-q* frame and the system *d-q* frame, due to the effect of the ac collection system, there also exists similar relationship between the WTG *d-q* frame and the common system *d-q* frame. As shown in Fig. 5, the voltage angle at the PCC is settled as zero which is defined as the common system *d-q* frame [35]. Each inverter is usually modeled and controlled in its own terminal *d-q* frame which is defined by its respective voltage deviation angle.

In this section, a simple method is used in which the alignment is achieved by a rotation matrix according to the WTG's respective voltage deviation angle. The method enables the use of *d-q* impedance models in their own local reference frame without any knowledge of the collection system. When all WTGs' impedance models are referred to the global reference frame, standard circuit analysis rules with impedance matrices can be applied. In this way, by referring all impedance matrices to a global reference frame, series and parallel connection rules are applicable. If the selected stability analysis is based on source and load impedance equivalents, a logical choice of global reference frame is the source/load interface point. Based on the Eq. (1), the transformation formula [35] in *d-q* domain is shown in Eqs. (17) and (18).

$$\boldsymbol{Z}'_{\text{wdq}} = \boldsymbol{T}_{\text{dq}} \boldsymbol{Z}_{\text{wdq}} \boldsymbol{T}_{\text{dq}}^{-1} \tag{17}$$

$$\boldsymbol{T}_{\mathrm{dq}}=\begin{bmatrix}\cos\theta_i & \sin\theta_i\\ -\sin\theta_i & \cos\theta_i\end{bmatrix} \tag{18}$$

where $\mathbf{Z}_{\mathrm{wdq}}$ represents the WTG's *d-q* impedance at its local reference frame, while $\mathbf{Z}$' wdq denotes the WTG's *d-q* impedance at the global reference frame.

By substituting the linearization transfer matrix derived in Eq. (13), the transformation formula in modified sequence domain is shown in Eqs. (19) and (20).

$$\boldsymbol{Z}'_{\mathrm{wpn}}=\boldsymbol{T}_{\mathrm{pn}}\boldsymbol{Z}_{\mathrm{wpn}}\boldsymbol{T}_{\mathrm{pn}}^{-1} \tag{19}$$

$$\boldsymbol{T}_{\mathrm{pn}}=\begin{bmatrix}e^{j\theta} & 0\\ 0 & e^{-j\theta}\end{bmatrix} \tag{20}$$

where $\boldsymbol{Z}_{\mathrm{wpn}}$ represents the WTG's modified sequence impedance at local reference frame, while $\boldsymbol{Z}$' wpn denotes the WTG's modified sequence impedance at global reference frame.

The impedance network of the wind farm is shown in Fig. 5(a), where impedances of the WTG, transmission lines and transformers have been converted to the high-voltage side. Based on the circuit theory, the i^{th} collection line's general equivalent impedance can be obtained in Eq. (21).

$$\begin{aligned}\boldsymbol{Z}^i_{\mathrm{W\_1}}&=\left((\boldsymbol{Z}_{\mathrm{wpn}\_i1}+\boldsymbol{Z}_{\mathrm{T\_1ow}}+\boldsymbol{Z}_{\mathrm{L\_w}})^{-1}+(\boldsymbol{Z}_{\mathrm{wpn}\_i2}+\boldsymbol{Z}_{\mathrm{T\_1ow}})^{-1}\right)^{-1}\\ \boldsymbol{Z}^i_{\mathrm{W\_2}}&=\left((\boldsymbol{Z}^i_{\mathrm{W\_1}}+\boldsymbol{Z}_{\mathrm{L\_w}})^{-1}+(\boldsymbol{Z}_{\mathrm{wpn}\_i3}+\boldsymbol{Z}_{\mathrm{T\_1ow}})^{-1}\right)^{-1}\\ &\vdots\\ \boldsymbol{Z}^i_{\mathrm{W}\_n_i-1}&=\left((\boldsymbol{Z}^i_{\mathrm{W}\_n_i-2}+\boldsymbol{Z}_{\mathrm{L\_w}})^{-1}+(\boldsymbol{Z}_{\mathrm{wpn}\_in_i}+\boldsymbol{Z}_{\mathrm{T\_1ow}})^{-1}\right)^{-1}\\ \boldsymbol{Z}^i_{\mathrm{W}}&=\boldsymbol{Z}^i_{\mathrm{W}\_n_i-1}+\boldsymbol{Z}_{\mathrm{L}\_i}(\mathrm{i}\in[1,m])\end{aligned} \tag{21}$$

Where $\mathbf{Z}$i W is the i^{th} collection line's general equivalent impedance; $Z_{\mathrm{L\_i}}$ is the impedance of the i^{th} transmission line; $Z_{\mathrm{L\_w}}$ is the impedance of the cable between WTGs.

The impedance of the load system can be represented in Eq. (22)

$$\begin{aligned}&\boldsymbol{Z}^{\mathrm{WF}}_{\mathrm{pn}}\\ &=\left((\boldsymbol{Z}^1_{\mathrm{W}})^{-1}+(\boldsymbol{Z}^2_{\mathrm{W}})^{-1}+(\boldsymbol{Z}^3_{\mathrm{W}})^{-1}+\cdots(\boldsymbol{Z}^i_{\mathrm{W}})^{-1}\cdots+(\boldsymbol{Z}^m_{\mathrm{W}})^{-1}\right)^{-1}\\ &\quad+\boldsymbol{Z}_{\mathrm{T\_high}}\end{aligned} \tag{22}$$

The impedance of the source system can be represented in (23).

$$\boldsymbol{Z}^{\mathrm{G}}_{\mathrm{pn}}=\boldsymbol{Z}_{\mathrm{inside}} \tag{23}$$

The above impedance is based on modified sequence domain which still needs the shift of the frequency axis to be transferred to the real sequence impedance. By substituting $s\to s-j\omega_1$ for positive sequence impedance, and $s\to s+j\omega_1$ for negative sequence impedance, the real sequence impedance can be gotten. Also, in the realistic impedance measurement, the positive- and negative- sequence impedance are usually gotten via the positive or negative series voltage injection. To compare with the frequency sweeping measurement, the SISO impedance needs to be derived. With the series voltage injection as shown in Fig. 5(b) and (c), the one-dimension SISO equivalent impedance of the wind farm can be obtained in Eqs. (24)–(26). The detailed derivation is shown in Appendix A.

$$Z^{\mathrm{WF}}_{\mathrm{p}}(s)\big|_{\mathrm{series}}=\frac{Z^{\mathrm{WF}}_{\mathrm{pp}}(s-j\omega_1)Z^{\mathrm{G}}_{\mathrm{nn}}(s-j\omega_1)-Z^{\mathrm{WF}}_{\mathrm{pn}}(s-j\omega_1)Z^{\mathrm{G}}_{\mathrm{np}}(s-j\omega_1)+D_{\mathrm{WF}}(s}{Z^{\mathrm{G}}_{\mathrm{nn}}(s-j\omega_1)+Z^{\mathrm{WF}}_{\mathrm{nn}}(s-j\omega_1)}$$

$$Z^{\mathrm{WF}}_{\mathrm{n}}(s)\big|_{\mathrm{series}}=\frac{Z^{\mathrm{WF}}_{\mathrm{nn}}(s+j\omega_1)Z^{\mathrm{G}}_{\mathrm{pp}}(s+j\omega_1)-Z^{\mathrm{WF}}_{\mathrm{pn}}(s+j\omega_1)Z^{\mathrm{G}}_{\mathrm{np}}(s+j\omega_1)+D_{\mathrm{WF}}(s}{Z^{\mathrm{G}}_{\mathrm{pp}}(s+j\omega_1)+Z^{\mathrm{WF}}_{\mathrm{pp}}(s+j\omega_1)}$$

$$D_{\mathrm{WF}}=Z^{\mathrm{WF}}_{\mathrm{pp}}Z^{\mathrm{WF}}_{\mathrm{nn}}-Z^{\mathrm{WF}}_{\mathrm{pn}}Z^{\mathrm{WF}}_{\mathrm{np}} \tag{26}$$

Now, the accurate aggregated modified sequence impedance model of the wind farm has been obtained and one-dimension SISO sequence impedance is also derived under series voltage injection.

4. Model analysis and validation

In this section, a scaled wind farm consisting of 11 permanent magnetic direct drive wind turbines is built on Matlab/Simulink environment referring to a realistic wind farm [11]. Despite that the scale of the studied wind farm is downsized, its complexity and completeness are sufficient to reflect dynamics of the real wind farm. Effects of different working conditions and internal interactions within the farm are taken into account in this simulation model. The topology of the studied wind farm is depicted in Fig. 5(d), whose electrical parameters are listed in Table 1 and Table 2. Three scenarios' comparisons between the analytical model and the simulation model are implemented, i.e., (1) single WTG; (2) WTGs receive same wind speed; (3) WTGs receive different wind speeds. What is more, the single-machine model of the wind farm is compared to the analytically derived accurate aggregated sequence impedance model proposed in this paper.

4.1. Impedance model validation for single WTG

Before verifying the aggregated sequence impedance model of the wind farm, the accuracy of the single WTG's impedance model has to be guaranteed. In this part, the single WTG is connected to the ideal grid directly, which means the grid impedance is decoupled with the WTG's impedance. Z_{Sim} represents the impedance acquired by frequency sweeping, while Z_{Ana} represents the impedance acquired by aggregate impedance model. As shown in Fig. 6, the analytical impedance curves are consistent with frequency scanning impedance curves, including magnitude and phase curves of positive and negative impedances. Therefore, the single WTG's impedance model has been verified which is accurate.

4.2. Impedance model validation for wind farm

4.2.1. WTGs receive same wind speed

In this part, the aggregated sequence impedance model of the wind farm is verified when all wind turbines receive identical incoming wind speed. Incoming wind speeds of WTGs are represented by respective equivalent active power input as shown in Table B1 in Appendix B. The first thing is to calculate power flow information which is listed in Table B1 in Appendix B. As shown in Fig. 7(a), the analytical impedance curves are consistent with frequency scanning impedance curves, including magnitude and phase curves of positive and negative impedances. The correctness of the accurate aggregated sequence impedance model is verified when all WTGs work on the same operation state.

Also, to prove the necessity of the aggregated sequence impedance model proposed in this paper, the single-machine model [5–7] is established as a comparison. It is advisable to apply the single-machine aggregated model when all wind turbines receive identical wind speed and work on the same condition. The single-machine model of the wind farm is identical to individual WTG model as shown in Fig. 1 employing the same electrical and mechanical parameters in per unit value under the respective machine bases. Such single-machine model is compared with the above verified accurate aggregated sequence im-

pedance model as shown in Fig. 7(b). Z_{Proposed} represents the impedance of the aggregate impedance model, while $Z_{\text{Single\_M}}$ represents the impedance of the single-machine model.

It can be observed that in low frequency range, there exists steady state error both in positive and negative sequence impedance magnitude curves. And this error is larger in high frequency range. The error in low frequency range mainly results from single-machine model's inaccurate equivalence of control parameters, which keep same in per unit value. Since the impedance of the collection system is not accurately modeled in the single-machine model, the error in high frequency is large. It can be concluded that the aggregated impedance model proposed in this paper is more accurate than the single-machine model.

4.2.2. WTGs receive different wind speeds

The model proposed in this paper has been verified in the above part when all WTGs receive identical incoming wind speed. However, in the realistic wind farm, the WTGs located in different collection lines usually work on different operation states due to the wind speed distribution's difference. The single-machine model is not able to consider this condition. To prove the universality of the accurate aggregated sequence impedance model derived above, in this part, the WTGs within the wind farm work at various wind speeds. Incoming wind speeds of WTGs are represented by respective equivalent active power input as shown in Table B2 in Appendix B.

The first step is still to implement the power flow calculation whose results are listed in Table 5 in Appendices. Compared with frequency scanning impedance curves, as shown in Fig. 7(c), the analytical impedance curves fit well, including magnitude and phase curves of positive and negative impedances. The accuracy and universality of such model has been proved when WTGs receive different incoming wind speeds.

The contrast between receiving same wind speed and different wind speeds has also been implemented via the accurate aggregated sequence impedance model. When WTGs operate under different wind speeds, the impedance comparison with the case in Section 4.2.1 is shown in Fig. 7(d). It can be observed that there exists significant difference in magnitude and phase curves of positive and negative impedances. The deviations of operation points affect each WTG's impedance and their interactions within the farm, which together lead to the change of the wind farm output impedance.

5. The application in stability analysis

In this section, the accurate aggregated sequence impedance model of the wind farm derived above is utilized to analyze the stability of the whole system under different SCR. What is more, the results are compared with that of the single-machine aggregated model. In terms of the stability judgement, time domain simulations of the studied wind farm are utilized to verify the accuracy of the aggregated sequence impedance model derived in this paper.

Stability conditions of the grid-tied wind farm system can be predicted by applying GNC [36] to the impedance ratio $\boldsymbol{L}$ between the grid impedance and the wind farm output impedance. It has been proved in Ref. [23] that when the GNC is applied to the *d-q* and the modified sequence domains, the results are identical. The complex sequence impedance ration $\boldsymbol{L}_{\text{pn}}$ between the grid impedance and the wind farm impedance is shown in Eq. (27).

$$\boldsymbol{L}_{\text{pn}} = \boldsymbol{Z}_{\text{pn}}^{\text{G}} \cdot \text{inv}(\boldsymbol{Z}_{\text{pn}}^{\text{WF}}) \tag{27}$$

Fig. 8 shows the comparison of the characteristic locus of the $\boldsymbol{L}_{\text{pn}}$ between the single-machine model and the accurate aggregated sequence impedance model under different SCR. Corresponding time domain simulation waveforms are also displayed in Fig. 8. As the SCR decreases, the characteristic loci $\lambda_{\text{Proposed\_p}}$ tends to encircle the critical point clockwise, which means the wind farm is destabilized with the lower grid impedance. To be specific, with SCR settled as 10 shown in Fig. 8(a), the characteristic locus $\lambda_{\text{Proposed\_p}}$ doesn't encircle the critical point (−1, 0), which means the grid-tied wind farm is stable. With SCR settled as 6.45, as shown in Fig. 8(b), the characteristic loci $\lambda_{\text{Proposed\_p}}$ encloses the critical point clockwise, which means the wind farm operates in critical state. With SCR settled as 4, from the Fig. 8(c) characteristic loci $\lambda_{\text{Proposed\_p}}$ encircles the critical point clockwise, which means the wind farm operates unstably in a weak grid. However, the characteristic locus $\boldsymbol{\lambda}_{\text{Single\_M}}$ shows a different result. There exists an error between the $\boldsymbol{\lambda}_{\text{Single\_M}}$ and $\boldsymbol{\lambda}_{\text{Proposed}}$. The distinctive difference could be observed especially in critical state, when the $\lambda_{\text{Proposed\_p}}$ has encircled the critical point (−1, 0) whereas $\lambda_{\text{Single\_M\_p}}$ still denotes the stability.

To verify the stability judgement results of the aggregate impedance model, time simulations of the studied wind farm are implemented under the above three SCR. With SCR settled as 10 shown in Fig. 8(a), the system operates stably with the constant power output and sinusoidal three phase voltage and current waveforms. With SCR settled as 6.45 shown in Fig. 8(b), the system operates at the critical state. It can be observed that the output active power and reactive power exhibit sustained amplitude oscillations. With SCR settled as 4 shown in Fig. 8(c), the system operates unstably with the appearance of increasing oscillations of the active and reactive power. It's evident that the above simulations fit well with the loci of the $\boldsymbol{\lambda}_{\text{Proposed}}$ which verify the correctness of the proposed accurate aggregate impedance model. It can be concluded that the single-machine model is not precise for wind farm stability analysis.

6. The effects of the inertial controller on stability analysis

With the increasing penetration of WTGs, the number of traditional plants is falling which requires WTGs to share frequency and voltage regulation tasks [37]. In order to perfect the aggregation method and stick to the current state of the art, the inertial controller is considered in the process of aggregation and its impacts on the stability of the power system are discussed.

6.1. Aggregation of the wind farm attached with the inertial controller

The principle of the inertial control is to let the WTG respond to the rate of change of the frequency. This feature is often referred to as "virtual inertia" effect, as it introduces an output power term proportional to $(df)/(dt)$ [37]. Generally, inertial control is incorporated in the individual WTG's controllers. Since this paper is focused on the small-signal stability, the inertia extracted from the PMSG can be set small compared to the total power output. In other words, the steady-state operating point will not be affected. The dead zone of the inertial controller becomes invalid which is neglected as shown in Fig. 9 [37]. Therefore, it's still reasonable to assume the wind power input (P_{W}) constant. The output of the inertial controller is directly superimposed on the P_{W} of the WTG. The value of the k_{inertia} is expressed in p.u. on the WT frequency modulation power base (2% of total power input). The derivation of the inertial controller in frequency domain is shown below.

$$\Delta P_{\text{ref}} = \Delta P_{\text{inertia}}^{\text{WT}} = k_{inertia} \cdot s \cdot \Delta f \tag{28}$$

$$\Delta f = \frac{1}{2\pi} \cdot s \cdot \Delta\theta = -\frac{1}{2\pi} \cdot (k_{\text{pPLL}} + \frac{k_{\text{iPLL}}}{s}) \cdot \Delta u_{\text{wq}}^{\text{c}} \tag{29}$$

In fact, the basic idea of the proposed aggregation method is to establish the sequence impedance model of each component within the farm and then simplify the impedance network based on the circuit theory. Therefore, it's only left to modify the sequence impedance model of the WTG with consideration of the inertial emulation controller. Under this circumstance, the dc current injected into the dc side of the converter will no longer maintain constant. The dc-side of the

WTG is modelled as follows.

$$I_{\mathrm{dcw0}} + \Delta I_{\mathrm{dcw}} = \frac{P_{\mathrm{ref0}} + \Delta P_{\mathrm{ref}}}{U_{\mathrm{dcw0}} + \Delta U_{\mathrm{dcw}}} \approx \frac{P_{\mathrm{ref0}}}{U_{\mathrm{dcw0}}} + \frac{\Delta P_{\mathrm{ref}}}{U_{\mathrm{dcw0}}} \tag{30}$$

$$\Delta I_{\mathrm{dcw}} = \frac{\Delta P_{\mathrm{ref}}}{U_{\mathrm{dcw0}}} \tag{31}$$

The dc dynamics of the main circuit (2) needs to be modified in the process of linearization.

$$\begin{aligned} s \cdot \Delta U_{\mathrm{dcw}} = & \begin{bmatrix} \frac{-V_{\mathrm{wd\_ref0}}}{C_{\mathrm{w}} U_{\mathrm{dcw0}}} & \frac{-V_{\mathrm{wq\_ref0}}}{C_{\mathrm{w}} U_{\mathrm{dcw0}}} & 0 \end{bmatrix} \\ & \cdot \begin{bmatrix} \Delta i^{\mathrm{s}}_{\mathrm{wd}} \\ \Delta i^{\mathrm{s}}_{\mathrm{wq}} \\ \Delta U_{\mathrm{dcw}} \end{bmatrix} - \begin{bmatrix} 0 & 0 & \frac{-1}{C_{\mathrm{w}}} \end{bmatrix} \cdot \begin{bmatrix} \Delta u^{\mathrm{s}}_{\mathrm{wd}} \\ \Delta u^{\mathrm{s}}_{\mathrm{wq}} \\ \Delta I_{\mathrm{dcw}} \end{bmatrix} \\ & + \begin{bmatrix} \frac{-I_{\mathrm{wd0}}}{C_{\mathrm{w}} U_{\mathrm{dcw0}}} & \frac{-I_{\mathrm{wq0}}}{C_{\mathrm{w}} U_{\mathrm{dcw0}}} \end{bmatrix} \cdot \begin{bmatrix} \Delta v^{\mathrm{s}}_{\mathrm{wd\_ref}} \\ \Delta v^{\mathrm{s}}_{\mathrm{wq\_ref}} \end{bmatrix} \end{aligned} \tag{32}$$

where the ΔI_{dcw} is no longer equal to zero. The mathematical model of the inertial controller derived above is integrated with the original WTG model (Eq. (7)). The aggregation procedure presented in Fig. 4 is repeated to acquire accurate aggregation model of the wind farm attached with inertial controller.

6.2. Model validation and the stability analysis

The grid-connected system wind farm under study is shown in Fig. 10. The configuration and parameters of the wind farm (WF) are the same as those shown in Fig. 5(d) except for an inertial control attached to each WTG. The wind farm attached with the inertial control is connected to the PCC together with the three-phase passive load (C_{load}: 0.25 mF R_{load}: 3 Ω L_{g}: 0.2 H).

As shown in Fig. 11(a), the analytical model's impedance curves are consistent with frequency scanning impedance curves, including magnitude and phase curves of positive and negative impedances. Therefore, the single WTG's impedance model with the inertial controller has been verified which is accurate. As shown in Fig. 11(b), the analytical model's impedance curves fit well with frequency scanning impedance curves. The correctness of the accurate aggregated sequence impedance model of the wind farm is verified when all WTGs are attached with the inertial controller. With the inertial controller, the impedance of the wind farm will decline which is easier to intersect with the grid impedance resulting in instability.

By adjusting the value of k_{inertial}, the impacts of the inertial controller on the system stability margin can be displayed intuitively. In Fig. 12, it can be observed that the positive sequence impedance of the wind farm ZWT p declines with the rising of the k_{inertial} and intersects with the grid impedance ZG p when the k_{inertial} is set as 66 p.u. The phase margin is nearly zero (180°–176.8°≈0°) and the instability happens at about 20 Hz. This phenomenon is verified by simulation: as shown in Fig. 13(a), PCC voltage and current begin to diverge when the k_{inertial} is raised from 50 p.u to 66 p.u. And the oscillation frequency of the PCC current is about 20 Hz, as shown in Fig. 13(b).

In conclusion, the inertia controller has negative impacts on the stability of the wind farm system. In essence, the differential link brought by the inertial control will amplify the small-signal disturbance resulting in the instability. From the point of enhancing the wind farm system stability, it is recommended to set the inertial gain low. In fact, the operator of the power system has to balance the stability requirement and the TSOs' demand to find out an optimal value of the inertial gain.

7. Conclusions

In this paper, an accurate aggregated modelling method in modified sequence domain for wind farm systems is introduced and verified by time domain simulations. By comparing the proposed aggregated model with the traditional single-machine aggreagted model, the necessity of this paper's work is explained. The differences among each WTG's operation point are included in the proposed model. Based on such model, it is observed that wind speed distribution influences the wind farm's impedance characteristics greatly. What is more, it can be concluded that the inertia controller has negative impacts on the stability of the wind farm system, which means the better dynamic frequency response, the less stability margin. In contrast to the eigenvalue-based model, the accurate aggregated modified sequence impedance model proposed in this paper has many advantages. Not only the accuracy of the wind farm is guaranteed to reflect all dynamics, but also the simplicity for stability analysis can be highlighted. The entire system can be just separated into two subsystems represented by two impedances: load (wind farm) and source (grid), which is convenient for system-level stability analysis and engineering surveying.

Funding

This work was supported by the National Natural Science Foundation of China under Grant 51837007.

Appendix A. SISO equivalent impedance

In this paper, the series voltage injection is selected to implement the impedance frequency scanning. The positive sequence impedance Z_{p} and the negative sequence impedance Z_{n} could be gotten via the positive and negative voltage injection respectively. The corresponding analytical expression of the Z_{p} could be solved via following set of equations for series voltage injection. In terms of the positive voltage injection, equivalent equations of the circuit in Fig. 5(b) and (c) can be expressed as Eq. (A1).

$$\begin{aligned} V^{\mathrm{WF}}_{\mathrm{p}} &= I^{\mathrm{WF}}_{\mathrm{p}} Z^{\mathrm{WF}}_{\mathrm{pp}} + I^{\mathrm{WF}}_{\mathrm{n}} Z^{\mathrm{WF}}_{\mathrm{pn}} \\ V^{\mathrm{WF}}_{\mathrm{n}} &= I^{\mathrm{WF}}_{\mathrm{p}} Z^{\mathrm{WF}}_{\mathrm{np}} + I^{\mathrm{WF}}_{\mathrm{n}} Z^{\mathrm{WF}}_{\mathrm{nn}} \\ V^{\mathrm{G}}_{\mathrm{p}} &= I^{\mathrm{G}}_{\mathrm{p}} Z^{\mathrm{G}}_{\mathrm{pp}} + I^{\mathrm{G}}_{\mathrm{n}} Z^{\mathrm{G}}_{\mathrm{pn}} \\ V^{\mathrm{G}}_{\mathrm{n}} &= I^{\mathrm{G}}_{\mathrm{n}} Z^{\mathrm{G}}_{\mathrm{np}} + I^{\mathrm{G}}_{\mathrm{n}} Z^{\mathrm{G}}_{\mathrm{nn}} \\ I^{\mathrm{WF}}_{\mathrm{p}} &= -I^{\mathrm{G}}_{\mathrm{p}} = I_p \\ I^{\mathrm{WF}}_{\mathrm{n}} &= -I^{\mathrm{G}}_{\mathrm{n}} = I_n \\ V^{\mathrm{G}}_{\mathrm{n}} &= V^{\mathrm{WF}}_{\mathrm{n}} \end{aligned} \tag{A1}$$

where the superscript WF denotes the wind farm subsystem, while the superscript G represents the grid subsystem. The one-dimension positive impedance ZWF p considering coupling between the wind farm and the grid is shown in (A2).

$$Z^{\mathrm{WF}}_{\mathrm{p}}\Big|_{\mathrm{series}} = \frac{V^{\mathrm{WF}}_{\mathrm{p}}}{I_{\mathrm{P}}} \tag{A2}$$

In terms of the negative voltage injection, the derivation of the one-dimension negative impedance ZWF n as shown in formulae (A3) is similar to the above and details are not given here.

$$Z^{\mathrm{WF}}_{\mathrm{n}}\Big|_{\mathrm{series}} = \frac{V^{\mathrm{WF}}_{\mathrm{n}}}{I_{\mathrm{n}}} \tag{A3}$$

Appendix B. Power flow information

When WTGs work at the same wind speed, results of power flow calculation are listed in Table B1. When WTGs work at different wind speeds, results of power flow calculation are listed in Table B2.

Appendix C. The definition of A, B, C, D

$$\boldsymbol{A} = -s \cdot m(lc)^{-1} \cdot \left(\left(\frac{b \cdot f}{s} + d \right) \cdot \left(I - \frac{g \cdot f}{s} \right)^{-1} \left(h - (I + n) \cdot m^{-1} \right) \right.$$

$$\boldsymbol{B} = -s \cdot m(lc)^{-1} \cdot \left(a + \frac{b \cdot e}{s} - s \cdot I - clm^{-1} + \left(\frac{b \cdot f}{s} + d \right) \cdot \left(I - \frac{g \cdot f}{s} \right)^{-1} \left(\frac{g \cdot e}{s} + \right. \right.$$

$$\boldsymbol{C} = -lm^{-1}\boldsymbol{D} = lm^{-1}$$

$$a = \begin{bmatrix} \frac{-R_w}{L_w} & \omega_0 \\ -\omega_0 & \frac{-R_w}{L_w} \end{bmatrix} b = \begin{bmatrix} \frac{V_{wd\_ref0}}{L_w U_{dcw0}} \\ \frac{V_{wq\_ref0}}{L_w U_{dcw0}} \end{bmatrix} c = \begin{bmatrix} \frac{1}{L_w} & 0 \\ 0 & \frac{1}{L_w} \end{bmatrix} d = \begin{bmatrix} \frac{1}{L_w} & 0 \\ 0 & \frac{1}{L_w} \end{bmatrix} e$$

$$f = \begin{bmatrix} \frac{-I_{wd0}}{C_w U_{dcw0}} & \frac{-I_{wq0}}{C_w U_{dcw0}} \end{bmatrix} g = \begin{bmatrix} -(k_{pi} + \frac{k_{ii}}{s}) \cdot (k_{pu} + \frac{k_{iu}}{s}) \\ 0 \end{bmatrix} h = \begin{bmatrix} -$$

$$l = \begin{bmatrix} 1 & \frac{1}{s} \cdot (k_{pPLL} + \frac{k_{iPLL}}{s}) \cdot U_{wq0} \\ 0 & 1 - \frac{1}{s} \cdot (k_{pPLL} + \frac{k_{iPLL}}{s}) \cdot U_{wd0} \end{bmatrix} m = \begin{bmatrix} 0 & \frac{1}{s} \cdot (k_{pPLL} + \frac{k_{iPLL}}{s}) \cdot I_{wq0} \\ 0 & -\frac{1}{s} \cdot (k_{pPLL} + \frac{k_{iPLL}}{s}) \cdot I_{wd0} \end{bmatrix} n$$

Appendix D. The derivation of the linear transformation

$$\begin{bmatrix} V_d \\ V_q \end{bmatrix} = \sqrt{\tfrac{3}{2}} V_p \begin{bmatrix} 1 \\ -j \end{bmatrix}, \omega_{dq} = \omega_p - \omega_1$$
$$\begin{bmatrix} V_p \\ V_n \end{bmatrix} = \sqrt{\tfrac{3}{2}} V_n \begin{bmatrix} 1 \\ j \end{bmatrix}, \omega_{dq} = \omega_n + \omega_1 \tag{A6}$$

$$\begin{bmatrix} V_d \\ V_q \end{bmatrix} = \begin{bmatrix} Z_{dd} & Z_{dq} \\ Z_{qd} & Z_{qq} \end{bmatrix} \begin{bmatrix} I_d \\ I_q \end{bmatrix} = \boldsymbol{Z}_{dq} \begin{bmatrix} I_d \\ I_q \end{bmatrix} \tag{A7}$$

$$V_p \begin{bmatrix} 1 \\ -j \end{bmatrix} + V_n \begin{bmatrix} 1 \\ j \end{bmatrix} = \boldsymbol{Z}_{dq} \left(I_p \begin{bmatrix} 1 \\ -j \end{bmatrix} + I_n \begin{bmatrix} 1 \\ j \end{bmatrix} \right) \tag{A8}$$

$$\boldsymbol{Z}_{pn} = \frac{1}{2} \begin{bmatrix} \begin{bmatrix} 1 & j \end{bmatrix} \boldsymbol{Z}_{dq} \begin{bmatrix} 1 \\ -j \end{bmatrix} & \begin{bmatrix} 1 & j \end{bmatrix} \boldsymbol{Z}_{dq} \begin{bmatrix} 1 \\ j \end{bmatrix} \\ \begin{bmatrix} 1 & -j \end{bmatrix} \boldsymbol{Z}_{dq} \begin{bmatrix} 1 \\ -j \end{bmatrix} & \begin{bmatrix} 1 & -j \end{bmatrix} \boldsymbol{Z}_{dq} \begin{bmatrix} 1 \\ j \end{bmatrix} \end{bmatrix} \tag{A9}$$

References

[1] K. Ohlenforst, S. Sawyer, A. Dutton, B. Backwell, R. Fiestas, "Global wind report 2018," global wind energy council (GWEC), Tech. Rep. (2018) http://www.gwec.net/.

[2] M. Amin, M. Molinas, Understanding the origin of oscillatory phenomena observed between wind farms and HVDC systems, IEEE J. Emerg. Sel. Top. Power Electron. 5 (March (1)) (2017) 378–392.

[3] M. Krpan, I. Kuzle, Introducing low-order system frequency response modelling of a future power system with high penetration of wind power plants with frequency support capabilities, IET Renew. Power Gener. 12 (October (13)) (2018) 1453–1461.

[4] Y. Wang, Y. Yuan, Inertia provision and small signal stability analysis of a wind-power generation system using phase-locked synchronized equation, Sustainability 11 (March (5)) (2019) 1400.

[5] L. Kunjumuhammed, B. Pal, C. Oates, K. Dyke, Electrical oscillations in wind farm systems: analysis and insight based on detailed modeling, Boston, MA, 2016 IEEE Power and Energy Society General Meeting (PESGM) (2016) 1.

[6] G. Tapia, A. Tapia, J.X. Ostolaza, Two alternative modeling approaches for the evaluation of wind farm active and reactive power performances, IEEE Trans. Energy Convers. 21 (December (4)) (2006) 909–920.

[7] Vladislav Akhmatov, H. Knudsen, An aggregate model of a grid-connected, large-scale, offshore wind farm for power stability investigations—importance of windmill mechanical system, Int. J. Electr. Power Energy Syst. 24 (9) (2002) 709–717.

[8] M.A. Chowdhury, N. Hosseinzadeh, M.M. Billah, S.A. Haque, Dynamic DFIG wind farm model with an aggregation technique, Dhaka, International Conference on Electrical & Computer Engineering (ICECE 2010) (2010) 330–333.

[9] N. Dhlamini, S.P. Chowdhury, The impact of wind farm aggregation techniques for analyzing power system dynamics, Stoke on Trent, 2015 50th International Universities Power Engineering Conference (UPEC) (2015) 1–6.

[10] A. Marinopoulos, et al., Investigating the impact of wake effect on wind farm aggregation, Trondheim, 2011 IEEE Trondheim PowerTech (2011) 1–5.

[11] L.P. Kunjumuhammed, B.C. Pal, C. Oates, K.J. Dyke, The adequacy of the present practice in dynamic aggregated modeling of wind farm systems, IEEE Trans. Sustain. Energy 8 (January (1)) (2017) 23–32.

[12] E. Muljadi, et al., Equivalencing the collector system of a large wind power plant, Montreal, Que, 2006 IEEE Power Engineering Society General Meeting (2006) 9.

[13] J. Brochu, C. Larose, R. Gagnon, Validation of single- and multiple-machine equivalents for modeling wind power plants, Detroit, MI, USA, 2011 IEEE Power and Energy Society General Meeting (2011) 1.

[14] R.D. Middlebrook, Input Filter Considerations in Design and Application of Switching Regulators, IAS, 1976.

[15] M. Cespedes, J. Sun, Impedance modeling and analysis of grid-connected voltage-source converters, IEEE Trans. Power Electron. 29 (March (3)) (2014) 1254–1261.

[16] B. Wen, D. Boroyevich, R. Burgos, P. Mattavelli, Z. Shen, Analysis of D-Q small-signal impedance of grid-tied inverters, IEEE Trans. Power Electron. 31 (January (1)) (2016) 675–687.

[17] J. Lyu, X. Zhang, X. Cai, M. Molinas, Harmonic state-space based small-signal impedance modeling of a modular multilevel converter with consideration of internal harmonic dynamics, IEEE Trans. Power Electron. 34 (March (3)) (2019) 2134–2148.

[18] A. Rygg, M. Molinas, C. Zhang, X. Cai, A modified sequence-domain impedance definition and its equivalence to the dq-domain impedance definition for the stability analysis of AC power electronic systems, IEEE J. Emerg. Sel. Top. Power Electron. 4 (December (4)) (2016) 1383–1396.

[19] M. Kazem Bakhshizadeh, et al., Couplings in phase domain impedance modeling of grid-connected converters, IEEE Trans. Power Electron. 31 (October (10)) (2016) 6792–6796.

[20] S. Shah, L. Parsa, Sequence domain transfer matrix model of three-phase voltage source converters, Boston, MA, 2016 IEEE Power and Energy Society General Meeting (PESGM) (2016) 1–5.

[21] G.C. Paap, Symmetrical components in the time domain and their application to power network calculations, IEEE Trans. Power Syst. 15 (May (2)) (2000) 522–528.

[22] D.N. Zmood, D.G. Holmes, G. Bode, Frequency domain analysis of three phase linear current regulators, Phoenix, AZ, USA, Conference Record of the 1999 IEEE Industry Applications Conference. Thirty-Forth IAS Annual Meeting (1999) 818–825, vol. 2.

[23] A. Rygg, M. Molinas, C. Zhang, X. Cai, On the equivalence and impact on stability of impedance modeling of power electronic converters in different domains, IEEE J. Emerg. Sel. Top. Power Electron. 5 (December (4)) (2017) 1444–1454.

[24] Mohamed Belkhayat, Stability Criteria for AC Power Systems With Regulated Loads, 1997.

[25] C. Zhang, X. Cai, A. Rygg, M. Molinas, Sequence domain SISO equivalent models of a grid-tied voltage source converter system for small-signal stability analysis, IEEE Trans. Energy Convers. 33 (June (2)) (2018) 741–749.

[26] H. Jiang, J. You, H. Liu, W. Ning, L. Wu, Impedance characteristics of DFIGs considering the impacts of DFIG numbers and locations and its application on SSR analysis, Chicago, IL, 2017 IEEE Power & Energy Society General Meeting (2017) 1–8.

[27] J. Lyu, X. Cai, M. Amin, M. Molinas, Sub-synchronous oscillation mechanism and its suppression in MMC-based HVDC connected wind farms, IET Gener. Transm. Distrib. 12 (February (4)) (2018) 1021–1029.

[28] M. Amin, A. Rygg, M. Molinas, Self-synchronization of wind farm in an MMC-based HVDC system: a stability investigation, IEEE Trans. Energy Convers. 32 (June (2)) (2017) 458–470.

[29] H. Liu, X. Xie, X. Gao, H. Liu, Y. Li, Stability analysis of SSR in multiple wind farms connected to series-compensated systems using impedance network model, IEEE Trans. Power Syst. 33 (May (3)) (2018) 3118–3128.

[30] A. Bonfiglio, M. Invernizzi, A. Labella, R. Procopio, Design and implementation of a variable synthetic inertia controller for wind turbine generators, IEEE Trans. Power Syst. 34 (January (1)) (2019) 754–764.

[31] A.B.T. Attya, J.L. Dominguez-García, Insights on the provision of frequency support by wind power and the impact on energy systems, IEEE Trans. Sustain. Energy 9 (April (2)) (2018) 719–728.

[32] H. Liu, et al., Subsynchronous interaction between direct-drive PMSG based wind farms and weak AC networks, IEEE Trans. Power Syst. 32 (November (6)) (2017) 4708–4720.

[33] C. Zhang, X. Cai, M. Molinas, A. Rygg, On the impedance modeling and equivalence of AC/DC side stability analysis of a grid-tied type-IV wind turbine system, IEEE Trans. Energy Convers. (2018).

[34] Z. Jenny Z, Impact of short circuit ratio and phase locked loop parameters on the small-signal behaviour of a VSC-HVdc converter, Boston, MA, 2016 IEEE Power and Energy Society General Meeting (PESGM) (2016) 1.

[35] A. Rygg, M. Molinas, E. Unamuno, C. Zhang, X. Cai, A Simple Method for Shifting Local Dq Impedance Models to a Global Reference Frame for Stability Analysis, June. Available: https://arxiv.org/abs/1706.08313, 2017.

[36] C.A. Desoer, Y.T. Wang, On the generalized nyquist stability criterion, Fort Lauderdale, FL, USA, 1979 18th IEEE Conference on Decision and Control Including the Symposium on Adaptive Processes (1979) 580–586.

[37] I.D. Margaris, S.A. Papathanassiou, N.D. Hatziargyriou, A.D. Hansen, P. Sorensen, Frequency control in autonomous power systems with high wind power penetration, IEEE Trans. Sustain. Energy 3 (April (2)) (2012) 189–199.